Letter

Beam spin asymmetry measurements of deeply virtual π^0 production with CLAS12

The CLAS Collaboration

A. Kim [a],*, S. Diehl [b,a], K. Joo [a], V. Kubarovsky [c], P. Achenbach [c], Z. Akbar [d,e,1], J.S. Alvarado [f], Whitney R. Armstrong [g], H. Atac [h], H. Avakian [c], C. Ayerbe Gayoso [i], L. Barion [j], M. Battaglieri [k], I. Bedlinskiy [l], B. Benkel [m], A. Bianconi [n,o], A.S. Biselli [p], M. Bondi [k], F. Bossù [q], S. Boiarinov [c], K.T. Brinkmann [b], W.J. Briscoe [r], W.K. Brooks [m], S. Bueltmann [s], V.D. Burkert [c], R. Capobianco [a], D.S. Carman [c], J.C. Carvajal [t], G. Charles [f,s], P. Chatagnon [c,f], V. Chesnokov [u], T. Chetry [t,v,w], G. Ciullo [j,x], B. Clary [a,2], G. Clash [y], P.L. Cole [z], M. Contalbrigo [j], G. Costantini [n,o], V. Crede [e], A. D'Angelo [aa,ab], N. Dashyan [ac], R. De Vita [k], M. Defurne [q], A. Deur [c], C. Dilks [ad], C. Djalali [w,ae], R. Dupre [f], H. Egiyan [c], M. Ehrhart [f,3], A. El Alaoui [m], L. El Fassi [v], S. Fegan [y], A. Filippi [af], C. Fogler [s], G. Gavalian [c], G.P. Gilfoyle [ag], G. Gosta [o], F.X. Girod [c], D.I. Glazier [ah], A.A. Golubenko [u], R.W. Gothe [ae], L. Guo [t], K. Hafidi [g], H. Hakobyan [m], M. Hattawy [s,g], F. Hauenstein [c,s], T.B. Hayward [a], D. Heddle [ai,c], A. Hobart [f], M. Holtrop [aj], Yu-Chun Hung [s], Y. Ilieva [ae], D.G. Ireland [ah], E. Isupov [u], H.S. Jo [ak], R. Johnston [al], S. Joosten [g,h], M. Khachatryan [s], A. Khanal [t], W. Kim [ak], V. Klimenko [a], A. Kripko [b], S.E. Kuhn [s], L. Lanza [aa,ab], M. Leali [n,o], M.L. Kabir [v], S. Lee [g], P. Lenisa [j,x], X. Li [al], I. .J.D. MacGregor [ah], D. Marchand [f], V. Mascagna [n,am,o], B. McKinnon [ah], D. Matamoros [f], S. Migliorati [n,o], T. Mineeva [m], M. Mirazita [an], V. Mokeev [c], P. Moran [al], C. Munoz Camacho [f], P. Naidoo [ah], K. Neupane [ae], D. Nguyen [c], S. Niccolai [f], G. Niculescu [ao], M. Osipenko [k], M. Ouillon [f], P. Pandey [s], M. Paolone [ap,h], L.L. Pappalardo [j,x], R. Paremuzyan [c,aj], E. Pasyuk [c], S.J. Paul [aq], W. Phelps [ai,r], N. Pilleux [f], M. Pokhrel [s], J. Poudel [s,4], J.W. Price [ar], Y. Prok [s], A. Radic [m], N. Ramasubramanian [q], Trevor Reed [t], J. Richards [a], M. Ripani [k], J. Ritman [as,5], P. Rossi [c,an], F. Sabatié [q], C. Salgado [at], S. Schadmann [as], A. Schmidt [r,al], Y.G. Sharabian [c], E.V. Shirokov [u], U. Shrestha [a,w], D. Sokhan [q,ah], N. Sparveris [h], M. Spreafico [k], S. Stepanyan [c], I.I. Strakovsky [r], S. Strauch [ae], J. Tan [ak], N. Trotta [a], R. Tyson [ah], M. Ungaro [c], S. Vallarino [j], L. Venturelli [n,o], H. Voskanyan [ac], E. Voutier [f], D.P. Watts [y], X. Wei [c], R. Wishart [ah], M.H. Wood [au], M. Yurov [v], N. Zachariou [y], J. Zhang [d], V. Ziegler [c], M. Zurek [g]

[a] University of Connecticut, Storrs, CT 06269, United States of America
[b] II Physikalisches Institut der Universitaet Giessen, 35392 Giessen, Germany
[c] Thomas Jefferson National Accelerator Facility, Newport News, VA 23606, United States of America
[d] University of Virginia, Charlottesville, VA 22901, United States of America
[e] Florida State University, Tallahassee, FL 32306, United States of America

* Corresponding author.
  E-mail address: andrey.kim@uconn.edu (A. Kim).
[1] Current address: National Research and Innovation Agency (BRIN), Indonesia.
[2] Current address: Lawrence Livermore National Laboratory, Livermore, CA 94550, United States of America.
[3] Current address: Argonne National Laboratory, Argonne, IL 60439, United States of America.
[4] Current address: Thomas Jefferson National Accelerator Facility, Newport News, VA 23606, United States of America.
[5] Current address: Ruhr-Universität Bochum, 44801 Bochum, Germany.

[f] *Université Paris-Saclay, CNRS/IN2P3, IJCLab, 91405 Orsay, France*
[g] *Argonne National Laboratory, Argonne, IL 60439, United States of America*
[h] *Temple University, Philadelphia, PA 19122, United States of America*
[i] *College of William and Mary, Williamsburg, VA 23187-8795, United States of America*
[j] *INFN, Sezione di Ferrara, 44100 Ferrara, Italy*
[k] *INFN, Sezione di Genova, 16146 Genova, Italy*
[l] *National Research Centre Kurchatov Institute - ITEP, Moscow, 117259, Russia*
[m] *Universidad Técnica Federico Santa María, Casilla 110-V Valparaíso, Chile*
[n] *Università degli Studi di Brescia, 25123 Brescia, Italy*
[o] *INFN, Sezione di Pavia, 27100 Pavia, Italy*
[p] *Fairfield University, Fairfield CT 06824, United States of America*
[q] *IRFU, CEA, Université Paris-Saclay, F-91191 Gif-sur-Yvette, France*
[r] *The George Washington University, Washington, DC 20052, United States of America*
[s] *Old Dominion University, Norfolk, VA 23529, United States of America*
[t] *Florida International University, Miami, FL 33199, United States of America*
[u] *Skobeltsyn Institute of Nuclear Physics, Lomonosov Moscow State University, 119234 Moscow, Russia*
[v] *Mississippi State University, Mississippi State, MS 39762-5167, United States of America*
[w] *Ohio University, Athens, OH 45701, United States of America*
[x] *Universitá di Ferrara, 44121 Ferrara, Italy*
[y] *University of York, York YO10 5DD, United Kingdom*
[z] *Lamar University, 4400 MLK Blvd, PO Box 10046, Beaumont, TX 77710, United States of America*
[aa] *INFN, Sezione di Roma Tor Vergata, 00133 Rome, Italy*
[ab] *Universitá di Roma Tor Vergata, 00133 Rome Italy*
[ac] *Yerevan Physics Institute, 375036 Yerevan, Armenia*
[ad] *Duke University, Durham, NC 27708-0305, United States of America*
[ae] *University of South Carolina, Columbia, SC 29208, United States of America*
[af] *INFN, Sezione di Torino, 10125 Torino, Italy*
[ag] *University of Richmond, Richmond, VA 23173, United States of America*
[ah] *University of Glasgow, Glasgow G12 8QQ, United Kingdom*
[ai] *Christopher Newport University, Newport News, VA 23606, United States of America*
[aj] *University of New Hampshire, Durham, NH 03824-3568, United States of America*
[ak] *Kyungpook National University, Daegu 41566, Republic of Korea*
[al] *Massachusetts Institute of Technology, Cambridge, MA 02139-4307, United States of America*
[am] *Università degli Studi dell'Insubria, 22100 Como, Italy*
[an] *INFN, Laboratori Nazionali di Frascati, 00044 Frascati, Italy*
[ao] *James Madison University, Harrisonburg, VA 22807, United States of America*
[ap] *New Mexico State University, PO Box 30001, Las Cruces, NM 88003, United States of America*
[aq] *University of California Riverside, 900 University Avenue, Riverside, CA 92521, United States of America*
[ar] *California State University, Dominguez Hills, Carson, CA 90747, United States of America*
[as] *GSI Helmholtzzentrum fur Schwerionenforschung GmbH, D-64291 Darmstadt, Germany*
[at] *Norfolk State University, Norfolk, VA 23504, United States of America*
[au] *Canisius College, Buffalo, NY, United States of America*

ARTICLE INFO

ABSTRACT

The new experimental measurements of beam spin asymmetry were performed for the deeply virtual exclusive π^0 production in a wide kinematic region with the photon virtualities Q^2 up to 6.6 GeV^2 and the Bjorken scaling variable x_B in the valence regime. The data were collected by the CEBAF Large Acceptance Spectrometer (CLAS12) at Jefferson Lab with longitudinally polarized 10.6 GeV electrons scattered on an unpolarized liquid-hydrogen target. Sizable asymmetry values indicate a substantial contribution from transverse virtual photon amplitudes to the polarized structure functions. The interpretation of these measurements in terms of the Generalized Parton Distributions (GPDs) demonstrates their sensitivity to the chiral-odd GPD $\bar{E}_T$, which contains information on quark transverse spin densities in unpolarized and polarized nucleons and provides access to the nucleon's transverse anomalous magnetic moment. Additionally, the data were compared to a theoretical model based on a Regge formalism that was extended to the high photon virtualities.

Deeply virtual meson electroproduction (DVMP) is one of the most effective ways to access Generalized Parton Distributions (GPDs), which are essential non-perturbative objects that provide extensive information on the 3D structure of hadrons [1–3]. DVMP processes at large photon virtuality can be factorized into a hard-scattering subprocess and a soft subprocess. For longitudinally polarized virtual photons at large photon virtuality Q^2 the factorization of this amplitude shown in Fig. 1 has been proven [2,4]. For transversely polarized virtual photons, a modified perturbative approach is used in current phenomenological models to take the parton transverse momenta into account as a higher-twist effect [5]. The hard subprocess can be calculated perturbatively and the soft parts of the convolution can be described with GPDs and a meson distribution amplitude (DA).

Previous experimental [7–23] and theoretical [5,6,24–26] studies of hard exclusive pseudoscalar meson electroproduction, especially π^0 and η electroproduction [5,6,12,13,16,17,27,28], have shown that the asymptotic leading-twist approximation is not sufficient to describe the experimental results from the existing measurements. It was found that there are strong contributions from transversely polarized virtual photons that have to be considered by including contributions from chiral-odd GPDs (H_T, $\tilde{H}_T$, E_T, and $\tilde{E}_T$) in addition to the chiral-even GPDs (H, $\tilde{H}$, E, and $\tilde{E}$), which depend on the momentum fraction of the parton x, the skewness ξ, and the four-momentum transfer to the nucleon t. π^0 meson production was shown to have an increased sensitivity to chiral-odd GPDs and is especially suited to constrain $\bar{E}_T = 2\tilde{H}_T + E_T$, due to the quark flavor composition.
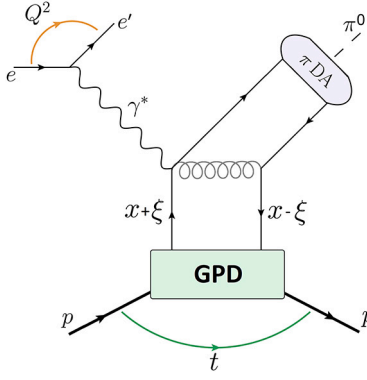
Fig. 1. Hard exclusive electroproduction of a pion on the proton in very forward kinematics ($-t/Q^2 \ll 1$), described by GPDs [5,6].

Fig. 2. Distributions of missing mass squared of the epX system before (black line) and after (red line) application of the exclusive constraints. The blue dashed lines represent the cuts on MM^2_{epX} that were also used for final exclusive $\vec{e}p \rightarrow e'p'\pi^0$ event selection.

The chiral-even GPDs can be related to the well-known nucleon form factors [6] but a few phenomenological constraints exist for the chiral-odd GPDs that cannot be accessed from the chiral-even sector. For example, the first moment of $\bar{E}_T$ can be interpreted as the proton's transverse anomalous magnetic moment [29], and in the forward limit, H_T becomes the transversity structure function h_1, which is directly related to the still unknown tensor charge of the nucleon [6,30].

An alternative description of hard exclusive pion production is provided by Laget (JML) model, which is based on Reggeized exchange of trajectories in the t-channel [31,32] and unitarity cuts [33,34]. While the Regge model starts at the real photon point and extends to the deeply virtual regime, a firm QCD foundation exists for the GPD model within the Bjorken regime and its applicability must be tested in the accessible Q^2 range. For a precise comparison to theoretical models and especially for a study of higher-twist effects, a study in $-t$, ϕ, x_B, and Q^2 with multidimensional binning is needed to reduce uncertainties and to access the kinematic dependencies of the GPDs involved, where Q^2 is the photon virtuality, x_B is the Bjorken scaling variable, t is the four-momentum transfer between the initial and final proton, and ϕ is the azimuthal angle between the electron scattering plane and the hadronic reaction plane in the center-of-mass frame.

In exclusive meson production experiments, GPDs are typically accessed through differential cross sections and beam and target polarization asymmetries [35–37]. In the one-photon exchange approximation the beam spin asymmetry (BSA) is defined as [35,36]:

$$BSA = \frac{\sqrt{2\epsilon(1-\epsilon)}\frac{\sigma_{LT'}}{\sigma_0}\sin\phi}{1+\sqrt{2\epsilon(1+\epsilon)}\frac{\sigma_{LT}}{\sigma_0}\cos\phi + \epsilon\frac{\sigma_{TT}}{\sigma_0}\cos 2\phi}, \quad (1)$$

where the structure functions σ_L and σ_T, which contribute to $\sigma_0 = \sigma_T + \epsilon\sigma_L$, correspond to coupling to longitudinal and transverse virtual photons, and ϵ describes the flux ratio of longitudinally and transversely polarized virtual photons. σ_{LT}, σ_{TT}, and the polarized structure function $\sigma_{LT'}$ describe the interference between their amplitudes. The focus of this work is on the extraction of the beam spin asymmetry moments related to the structure function ratio $\sigma_{LT'}/\sigma_0$.

For the present study, hard exclusive π^0 electroproduction was measured at Jefferson Lab with CLAS12 (CEBAF Large Acceptance Spectrometer for operation at 12 GeV) [38]. Beam spin asymmetries in forward kinematics were extracted over a wide range in Q^2, x_B and ϕ. The longitudinally polarized incident electron beam had an energy of 10.6 GeV with an average current of 40-55 nA, impinging on a 5-cm-long unpolarized liquid-hydrogen target placed at the center of the solenoid magnet of CLAS12. The large acceptance of the CLAS12 detector allowed simultaneous detection of all four final state particles of the $\vec{e}p \rightarrow e'p'\pi^0$ reaction, with the π^0 reconstructed by measuring the 2γ decay channel. The scattered electron was identified in the forward detector using the track reconstructed in the drift chambers (DC) and matching it with signals in a lead-scintillator electromagnetic sampling
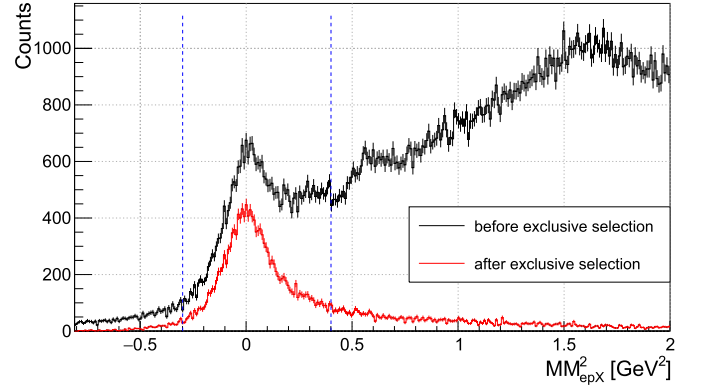
calorimeter (EC) and Cherenkov counter. The proton was identified as a positively charged particle track in the DC with the time-of-flight measurements from the scintillator counters. The neutral pion decay photons were detected using the EC energy and timing information.

For the selection of deeply inelastic scattered electrons, cuts on $Q^2 > 2\,\text{GeV}^2$ and on the invariant mass of the hadronic final state $W > 2$ GeV, were applied. The events with exactly one electron, one proton and at least two photons were selected as candidates for the exclusive $\vec{e}p \rightarrow e'p'\pi^0$ final state. With the 4-momenta reconstructed for all final state particles, the event kinematics is fully known, and energy and momentum conservation can be used to develop cuts to ensure exclusivity of the reconstructed events. These constraints reject the backgrounds from different channels (*e.g.* η, ρ or ω meson production) and from reactions with any additional undetected particle present. The exclusivity cuts were based on the following variables:

- $|\Delta P_T| < 0.3$ GeV and $-0.5 < \Delta P_z < 0.9$ GeV - missing transverse and longitudinal momenta of the $e'p'\gamma\gamma$ system;
- $|\Delta\phi_{X\pi}| < 4°$ - the difference between the azimuthal angles of the reconstructed and computed π^0 using the beam, target, and reconstructed e' and p' particles, peaked around zero;
- $-0.3 < MM^2_{epX} < 0.4$ GeV^2 - missing mass squared of $ep \rightarrow ep'X$ with the distribution peaked around the neutral pion mass squared.

Each exclusive variable distribution was fit and the experimental resolution σ was observed from the fit, the events within a $\pm 3\sigma$ range from the expected peak values were chosen as the final exclusive candidates. Fig. 2 illustrates the effect of the ΔP_T, ΔP_z, and $\Delta\phi_{X\pi}$ cuts on the missing mass squared of the epX system and demonstrates the power of these exclusive constraints to achieve clean $\vec{e}p \rightarrow e'p'\pi^0$ event selection.

After application of all exclusivity cuts, the invariant mass of two photons was used to estimate the remaining background from accidental photons using the sideband method. The observed background was found to be very small for all multidimensional bins, two of which are shown in Fig. 3. As a cross-check, the $M_{\gamma\gamma}$ distributions were fit with a Gaussian (describing the signal) plus a first-order polynomial (describing the background). The background estimate using the fit method was found to be consistent with the result from the sideband subtraction method, and was used to estimate the systematic uncertainty of the background subtraction.

The BSA was determined experimentally from the number of signal counts with positive and negative helicity ($N_i^{\pm}$), in a specific bin i as:

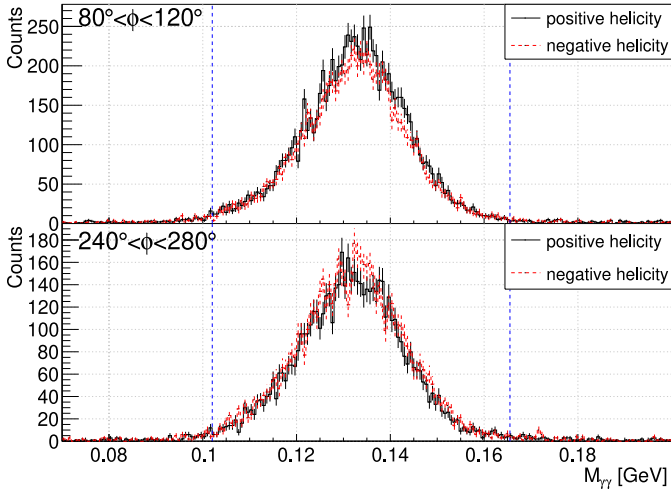$$BSA_i = \frac{1}{P_e}\frac{N_i^+ - N_i^-}{N_i^+ + N_i^-}, \quad (2)$$

Fig. 3. The invariant mass spectra of two decay photons show distributions peaked at the neutral pion mass. The plots for two opposite ϕ bins are shown on top ($80° < \phi < 120°$) and bottom ($240° < \phi < 280°$). Both plots are from the third $-t$ bin of fifth Q^2, x_B bin. The black solid histogram corresponds to the events with positive helicity and the red dashed histogram corresponds to the events with negative helicity. The blue dashed lines represent 3σ cuts on the invariant mass of two photons. The events outside of these lines are used for sideband subtraction to estimate the background, which is at the level of a few percent in all kinematic bins.

where P_e is the average magnitude of the beam polarization. P_e was measured with a Møller polarimeter upstream of CLAS12 to be 86.3%±2.6%. To obtain the signal counts, the $M_{\gamma\gamma}$ distribution for each multidimensional bin in Q^2, x_B, $-t$, and ϕ and for each helicity state was analyzed separately, and the background counts were subtracted using the sideband method, as described above. Fig. 4 shows the Q^2 versus x_B distribution of the exclusive events, together with the binning scheme applied for the multidimensional study. The size of binning grid was influenced by available statistics and aimed to offer a distinct kinematic representation of experimental measurements in a multi-dimensional space comparable with the measurements of exclusive deeply virtual π^+ production channel from CLAS12 [23]. The statistical uncertainty of the beam spin asymmetry was calculated based on standard error propagation. For each of the five $\{Q^2, x_B\}$ bins, three bins in $-t$ and nine equidistant bins in ϕ were defined to extract the BSA. Applying the same analysis procedure, the measurements were performed for two independent datasets with different experimental conditions, and the table with results can be found in the supplemental material. The bin sizes for each kinematic variable are greater than their respective resolutions.

To access the structure function ratio $\sigma_{LT'}/\sigma_0$, the BSA was plotted as a function of the azimuthal angle ϕ. Fig. 5 shows the BSA as a function of ϕ in two exemplar $-t$ bins for two different $Q^2 - x_B$ bin. As expected, the ϕ-dependence can be well described by Eq. (1). The denominator terms were fixed using the model parameterizations of the unpolarized structure functions measured by CLAS [11]. The impact of these terms in Eq. (1) on $\sigma_{LT'}/\sigma_0$ was studied using different parameterization values for the unpolarized structure functions and was found to be much smaller than the statistical uncertainty.

The extraction of the BSAs for the exclusive $\vec{e}p \rightarrow e'p'\pi^0$ channel includes several sources of systematic uncertainty. Above we have discussed the contribution from the background subtraction, evaluated by using two different methods to estimate the background counts from the invariant mass distribution of the two decay photons. The variations between asymmetries extracted using these two methods were 0.006 on average and were considered as systematic uncertainties. The systematic effect due to the uncertainty of the beam polarization was determined to be around 0.003 based on the uncertainty of the measure-
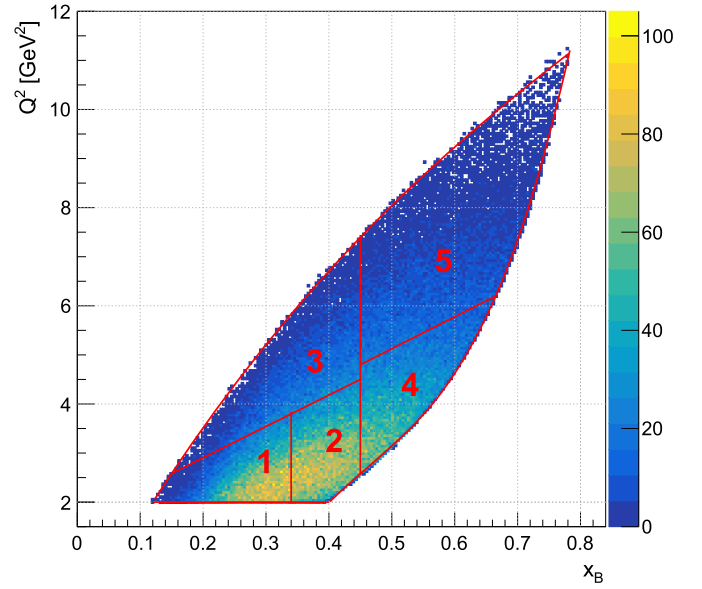

Fig. 4. Distribution of Q^2 versus x_B. The red lines represent the bin boundaries, and the bin numbering is given.
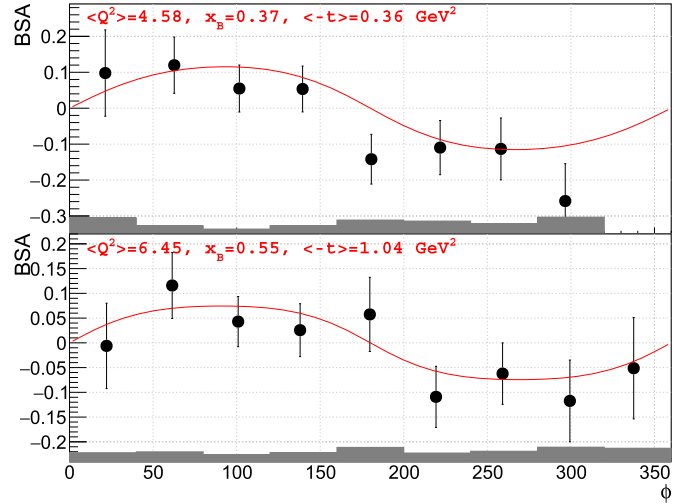

Fig. 5. Beam spin asymmetry as a function of ϕ for two representative kinematic bins. The vertical error bars show the statistical uncertainty of each point. The gray bands represent systematic uncertainties of the BSA measurements. The red lines show the fit with functional form of Eq. (1).

ment with the Møller polarimeter. A Geant4 Monte Carlo simulation was performed to estimate the impact of acceptance effects. This simulation included the CLAS12 detector response and generated asymmetries based on experimental values. The impact was evaluated by comparing the modeled and reconstructed asymmetries, and was found to be on the order of 0.013. Also bin migration effects and radiative effects were studied based on Monte Carlo simulations and estimated to be around 0.002. Additionally, for the systematic uncertainty associated with the event selection procedure, the exclusivity cuts were varied, and the corresponding BSA variations were estimated to be 0.014 on average. As mentioned above, the effect of the denominator terms from Eq. (1) on the fit results was also studied and estimated to be around 0.005. The individual systematic uncertainties were combined in quadrature, and the total uncertainty was conservatively estimated at 0.015 on average, which is smaller than the statistical uncertainty in most kinematic bins. Similarly, each individual source of systematic uncertainty was propagated to the extraction of $\sigma_{LT'}/\sigma_0$, and their combined values are shown on Fig. 6 as shaded band.
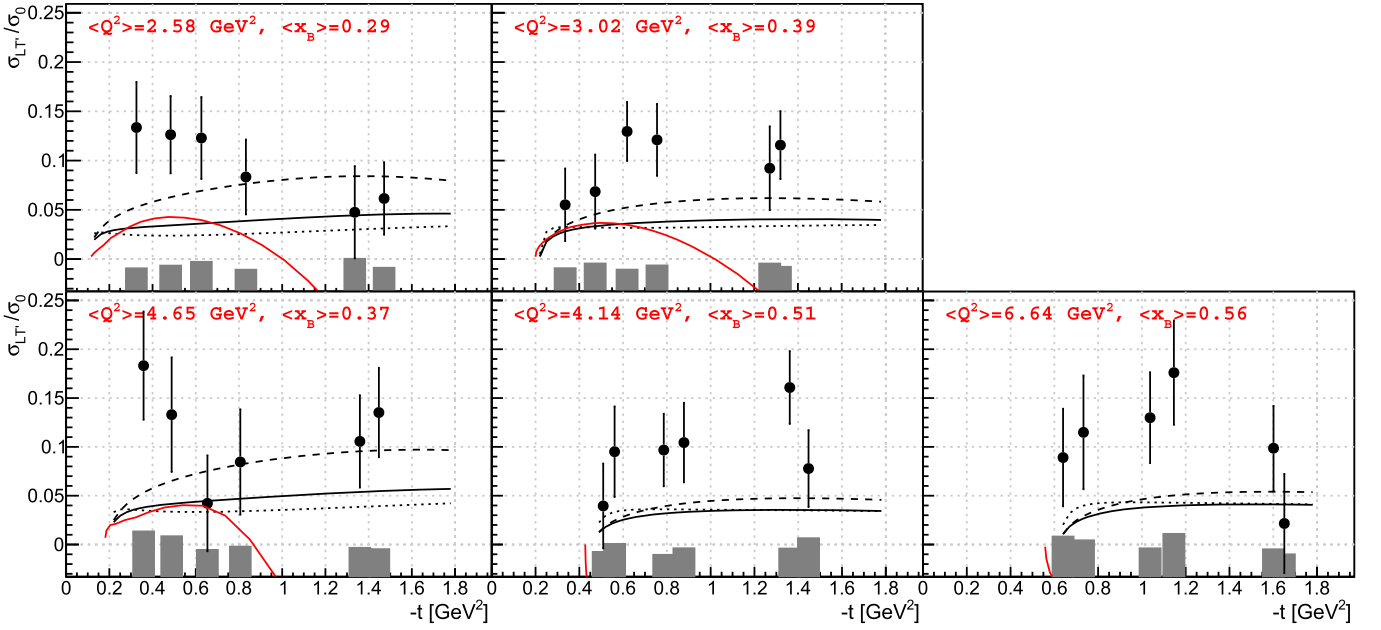
Fig. 6. The measurements of $\sigma_{LT'}/\sigma_0$ and its statistical uncertainty as a function of $-t$ in the forward kinematic regime. The gray bins represent the systematic uncertainties. The black curves show the theoretical prediction from the GPD-based Goloskokov-Kroll model. The black dashed lines show the effect of the GPD $\bar{E}_T$ multiplied by a factor of 0.5, and the black dotted lines show the effect of the GPD H_T multiplied by a factor 0.5. The red curve shows the theoretical predictions from the Regge-based JML model.

Fig. 6 shows the final results for the BSA moments extracted in the region of $-t$ up to 1.6 GeV^2 for the five $\{Q^2, x_B\}$ bins $(-t/Q^2 \approx 0.2 - 0.4)$, where the leading-twist GPD framework is applicable. It includes the comparison to the theoretical predictions from the GPD-based model by Goloskokov and Kroll (GK) [39] and the Regge-based JML model [31,32]. The structure function ratio $\sigma_{LT'}/\sigma_0$ is clearly positive in all kinematic bins and shaped by the contributing structure functions. The non-ϕ-dependent cross section $\sigma_0 = \sigma_T + \epsilon\sigma_L$ is determined by the interplay between the $\bar{E}_T$ and H_T contributions in the low $-t$ region, while $\sigma_{LT'}$ is constrained to be zero at $-t_{min}$ due to angular momentum conservation.

The GK model includes chiral-odd GPDs to calculate the contributions from the transversely polarized virtual photon amplitudes, with their t-dependence incorporated from Regge phenomenology. The GPDs are constructed from double distributions and constrained by the latest results from lattice QCD and transversity parton distribution functions [39]. A special emphasis is given to the GPDs H_T and $\bar{E}_T = 2\tilde{H}_T + E_T$, while contributions from other chiral-odd GPDs are neglected in the calculations, unlike chiral-even GPDs. $\sigma_{LT'}$ can be expressed through the convolutions of GPDs with subprocess amplitudes (twist-2 for the longitudinal and twist-3 for the transverse amplitudes) and contains the products of chiral-odd and chiral-even terms [5]:

$$\sigma_{LT'} \sim \xi\sqrt{1-\xi^2}\frac{\sqrt{-t'}}{2m}Im[\langle\bar{E}_T\rangle^*\langle\tilde{H}\rangle + \langle H_T\rangle^*\langle\tilde{E}\rangle]. \quad (3)$$

After expanding the dominating chiral-odd denominator term [5], the structure function ratio $\sigma_{LT'}/\sigma_0$ can be expressed by:

$$\frac{\sigma_{LT'}}{\sigma_0} \sim \frac{Im[\langle\bar{E}_T\rangle^*\langle\tilde{H}\rangle + \langle H_T\rangle^*\langle\tilde{E}\rangle]}{(1-\xi^2)|\langle H_T\rangle|^2 - \frac{t'}{8m^2}|\langle\bar{E}_T\rangle|^2 + \epsilon\sigma_L}. \quad (4)$$

Due to the quark flavor composition of the pions, π^0 production is typically dominated by $\bar{E}_T$, while the contribution from H_T is significantly smaller. In contrast, π^+ electroproduction shows a significantly stronger contribution from H_T. Since chiral even GPDs are much better known than their chiral odd counterparts, the strongest uncertainty for the theoretical prediction is expected from the so far poorly known GPD $\bar{E}_T$.

The comparisons between the experimental results and theoretical calculations demonstrate the difficulty to parameterize the delicate interference structure function $\sigma_{LT'}$ and estimate its sizable magnitude. The JML model shows positive values for the beam spin asymmetries in the three lowest x_B (close to 0.35) and Q^2 (below 4.5 GeV^2) bins for the low $-t$ regions, but fails to extrapolate to the two highest x_B and Q^2 bins. This model incorporates the dominant contributions which successfully build the unpolarized cross section. However, smaller contributions which are neglected may become relevant in BSA through their interference. For instance, the model does not include the real principal part of the rescattering amplitudes but takes into account only its singular part which provides the necessary imaginary part of the amplitude, and therefore a non-vanishing BSA. This conjecture, as well as the contributions of less likely intermediate states, remain to be investigated. The GK model provides a better description of the experimental measurements in a wide Q^2 and $-t$ range, but still predicts significantly smaller values for $\sigma_{LT'}/\sigma_0$. This discrepancy between the GK predictions and the experimental data might be explained by the interplay between the magnitudes of the chiral-odd GPDs H_T and $\bar{E}_T$. Based on Eq. (3) the results especially hint that $\bar{E}_T$ is overestimated. To illustrate the sensitivity of $\sigma_{LT'}/\sigma_0$ on the GPD $\bar{E}_T$, Fig. 6 also contains calculations with the GPD $\bar{E}_T$ reduced by an overall factor of 2 (black dashed line) and with the GPD H_T reduced by a factor 2 (black dotted line). The modification of the GPD $\bar{E}_T$ generates substantially larger BSA values, whereas the reduction of the GPD H_T shows a significantly smaller effect. This disparity reflects the dominance of the GPD $\bar{E}_T$ in the theoretical description of π^0 electroproduction, which makes it the most relevant channel to constrain $\bar{E}_T$. These effects are especially evident for the lower Q^2 bins, while the increase in the high Q^2 bins is noticeably smaller, which can indicate that the contributions of chiral-odd GPDs are still significant at the range of Q^2 accessible in CLAS12, and should be improved in the GK model calculations.

While a change of $\bar{E}_T$ helps as far as the description of $\sigma_{LT'}/\sigma_0$ is concerned, the consequences for other observables remain to be checked. This includes the measurements that show strong contributions from the transversity GPDs and need to be considered for the determination of $\bar{E}_T$, such as unpolarized cross section measurements for deeply virtual π^0 production from CLAS [8,11,12,16,17],

Hall A [18–20], COMPASS [21], and observables with transversely polarized targets for hard exclusive π^+ production from HERMES [39]. Altogether, a new global fit of the GPDs to all existing data from CLAS and Hall A, as well as the aforementioned HERMES and COMPASS results, and additional upcoming CLAS12 results on other mesons, becomes necessary. Here, the new multidimensional precision π^0 BSA data from this work and its high sensitivity to the GPD $\bar{E}_T$ will allow a better determination of this so far poorly known GPD. Based on the improvements in the knowledge of $\bar{E}_T$, it will become possible to improve the knowledge of the nucleon's anomalous magnetic moment $k_T^{u,d} = \int dx \bar{E}_T^{u,d}(x, \xi, t = 0)$, which is a fundamental quantity and so far only poorly constrained using lattice QCD results.

In summary, we have performed a multidimensional study of the BSA measurements for $\vec{e}p \to e'p'\pi^0$ at large photon virtuality, above the resonance region. In very forward kinematics, the magnitude of $\sigma_{LT'}/\sigma_0$ is underestimated in all Q^2 and x_B bins by the most advanced GPD-based model [39], indicating that a global fit of the model to existing experimental data is necessary to achieve an improved parameterization of the chiral odd GPDs, especially the dominating GPD $\bar{E}_T$.

Declaration of competing interest

The authors declare that they have no known competing financial interests or personal relationships that could have appeared to influence the work reported in this paper.

Data availability

Data will be made available on request.

Acknowledgements

Appendix A. Supplementary material

Supplementary material related to this article can be found online at https://doi.org/10.1016/j.physletb.2024.138459.

References

[1] A.V. Radyushkin, Phys. Rev. D 56 (1997) 5524.
[2] J.C. Collins, L. Frankfurt, M. Strikman, Phys. Rev. D 56 (1997) 2982.
[3] S.J. Brodsky, L. Frankfurt, J.F. Gunion, A.H. Mueller, M. Strikman, Phys. Rev. D 50 (1994) 3134.
[4] A. Radyushkin, Phys. Lett. B 385 (1996) 333.
[5] S. Goloskokov, P. Kroll, Eur. Phys. J. A 47 (2011) 112, arXiv:1106.4897 [hep-ph].
[6] G.R. Goldstein, J.O.G. Hernandez, S. Liuti, Phys. Rev. D 91 (2015) 114013.
[7] A. Airapetian, et al., Phys. Lett. B 535 (2002) 85.
[8] R. De Masi, et al., CLAS Collaboration, Phys. Rev. C 77 (2008) 042201.
[9] A. Airapetian, et al., Phys. Lett. B 659 (2008) 486.
[10] A. Airapetian, et al., Phys. Lett. B 682 (2010) 345.
[11] I. Bedlinskiy, et al., CLAS Collaboration, Phys. Rev. Lett. 109 (2012) 112001.
[12] I. Bedlinskiy, et al., CLAS Collaboration, Phys. Rev. C 90 (2014) 025205.
[13] A. Kim, et al., Phys. Lett. B 768 (2017) 168.
[14] P.E. Bosted, et al., CLAS Collaboration, Phys. Rev. C 95 (2017) 035207.
[15] P.E. Bosted, et al., CLAS Collaboration, Phys. Rev. C 95 (2017) 035206.
[16] I. Bedlinskiy, et al., CLAS Collaboration, Phys. Rev. C 95 (2017) 035202.
[17] B. Zhao, et al., Phys. Lett. B 789 (2019) 426.
[18] E. Fuchey, A. Camsonne, C. Munoz Camacho, M. Mazouz, G. Gavalian, et al., Phys. Rev. C 83 (2011) 025201, arXiv:1003.2938 [nucl-ex].
[19] M. Defurne, et al., Jefferson Lab Hall A Collaboration, Phys. Rev. Lett. 117 (2016) 262001.
[20] M. Mazouz, et al., Jefferson Lab Hall A Collaboration, Phys. Rev. Lett. 118 (2017) 222002.
[21] M.G. Alexeev, et al., COMPASS, Phys. Lett. B 805 (2020) 135454, arXiv:1903.12030 [hep-ex].
[22] S. Diehl, Prog. Part. Nucl. Phys. 133 (2023) 104069.
[23] S. Diehl, et al., Phys. Lett. B 839 (2023) 137761.
[24] M. Diehl, W. Kugler, Eur. Phys. J. C 52 (2007) 933, arXiv:0708.1121 [hep-ph].
[25] G. Duplancic, D. Muller, K. Passek-Kumericki, Phys. Lett. B 771 (2017) 603.
[26] M. Siddikov, I. Schmidt, Phys. Rev. D 99 (2019) 116005.
[27] S. Ahmad, G.R. Goldstein, S. Liuti, Phys. Rev. D 79 (2009) 054014, arXiv:0805.3568 [hep-ph].
[28] G.R. Goldstein, J.O. Hernandez, S. Liuti, Phys. Rev. D 84 (2011) 034007, arXiv:1012.3776 [hep-ph].
[29] M. Burkardt, Phys. Lett. B 639 (2006) 462.
[30] L. Gamberg, M. Malda, J.A. Miller, D. Pitonyak, A. Prokudin, N. Sato, Jefferson Lab Angular Momentum (JAM) Collaboration, Phys. Rev. D 106 (2022) 034014.
[31] J. Laget, Prog. Part. Nucl. Phys. 111 (2020) 103737.
[32] J.M. Laget, Phys. Rev. C 104 (2021) 025202, arXiv:2104.13078 [hep-ph].
[33] J.M. Laget, Phys. Lett. B 685 (2010) 146, arXiv:0912.1942 [hep-ph].
[34] J. Laget, Phys. Lett. B 695 (2011) 199.
[35] D. Drechsel, L. Tiator, J. Phys. G 18 (1992) 449.
[36] T. Arens, O. Nachtmann, M. Diehl, P.V. Landshoff, Z. Phys. C 74 (1997) 651, arXiv:hep-ph/9605376.
[37] M. Diehl, S. Sapeta, Eur. Phys. J. C 41 (2005) 515, arXiv:hep-ph/0503023.
[38] V.D. Burkert, et al., Nucl. Instrum. Methods A 959 (2020) 163419.
[39] S.V. Goloskokov, P. Kroll, Eur. Phys. J. C 65 (2010) 137, arXiv:0906.0460 [hep-ph].